The IMF to Planetary Masses Across the Milky Way

Scientific Category:	Stellar Physics
Scientific Keywords:	Astrometry, Brown Dwarfs, Interstellar Medium, Molecular Clouds, Pre-Main Sequence Stars
Alternate Category:	Stellar Populations
Instruments:	WFC3
Proprietary Period:	0 months

Proposal Size: Large JWST Initiative Yes

Orbit Request	Prime	Parallel
Cycle 25	132	0

Abstract

Observations have now verified the long-held theoretical assumption that the IMF extends into the planetary mass regime with the discovery of a small number of brown dwarfs as light as 5 MJup or below. Planetary-mass BDs are an extreme outcome of star formation, posing a strong test of the physics and conditions (e.g., gas density, turbulence, and temperature). There are strong theoretical arguments that the IMF should vary if these conditions change with environment, but this possibility remains untested since planetary-mass BDs have only been found in sparse associations. We propose to exploit a new fast-mosaic technique with WFC3/IR to map five benchmark star-forming regions that are more massive than any in the solar neighborhood; this survey will extend our census down the IMF into the planetary mass regime (3-5 MJup) and across environment from sparse associations (N=200) to massive clusters (N=50,000). We will map these clusters with three filters (F110W, F139M, F160W), exploiting water absorption in F139M to distinguish cool cluster members from reddened early-type field interlopers. In addition to identifying the bottom half of the IMF (0.5 Msun to 5 MJup) and measuring its slope and lowest extreme, we also will identify thousands of brown dwarfs (>1000 of which will fall below 15 MJup) for highly multiplexed JWST spectroscopy. Given the density of these clusters and extreme sensitivity but high overheads of JWST, multiplexed observations of dense cluster populations will yield the vast majority of spectra for free-floating exoplanet analogs over the next decade.

Investigators:

	Investigator	Institution	Country
	K Allers	Bucknell University	USA/PA
*	B Biller	University of Edinburgh, Institute for Astronomy	GBR
	B Bowler	University of Texas at Austin	USA/TX
	T Dupuy	University of Texas at Austin	USA/TX
*	C Fontanive	Royal Observatory Edinburgh	GBR
	K Kratter	University of Arizona	USA/AZ
	A Kraus	University of Texas at Austin	USA/TX
	J Lu	University of California - Berkeley	USA/CA
	S Offner	University of Massachusetts - Amherst	USA/MA
	M Reiter	University of Michigan	USA/MI
	A Rizzuto	University of Texas at Austin	USA/TX

Number of investigators: 11

* ESA investigators: 2

Target Summary:

Target	RA	Dec	Magnitude
RCW49+WESTERLUND2	10 23 58.1000	-57 45 49.20	V = 15 +/- 10
M16EAGLENEBULA	18 18 48.0000	-13 48 24.00	V = 15 +/- 5
M17	18 20 47.0000	-16 10 18.00	V = 15 +/- 10
W3-MAIN-OH	02 27 4.1000	+61 52 27.10	V = 15 +/- 10
CARINANEBULA	10 45 10.0000	-59 43 0.00	V = 15 +/- 10

Observing Summary:

Target	Config Mode and Spectral Elements	Flags	Orbits
RCW49+WESTERLUND2	WFC3/IR Imaging F160W		17
	WFC3/IR Imaging F110W		
	WFC3/IR Imaging F139M		
M16EAGLENEBULA	WFC3/IR Imaging F160W		26
	WFC3/IR Imaging F110W		
	WFC3/IR Imaging F139M		
M17	WFC3/IR Imaging F160W		30
	WFC3/IR Imaging F110W		

Target	Config Mode and Spectral Elements	Flags	Orbits
	WFC3/IR Imaging F139M		
W3-MAIN-OH	WFC3/IR Imaging F160W		34
	WFC3/IR Imaging F110W		
	WFC3/IR Imaging F139M		
CARINANEBULA	WFC3/IR Imaging F160W		25
	WFC3/IR Imaging F110W		
	WFC3/IR Imaging F139M		

Total prime orbits: 132

Scientific Justification

The Extreme Limit and Variations of the IMF

Over the past decade, observations have verified the long-held theoretical prediction that the IMF extends well into the planetary-mass regime (Low & Lynden-Bell 1976). The nearest young populations host brown dwarfs down to $\lesssim 10 M_{Jup}$ (e.g., Luhman et al. 2009b; Lodieu et al. 2013; Muzic et al. 2015; Kellogg et al. 2016; see Bastian et al. 2010 and Figure 1), and old, very cool analogs of these planetary-mass brown dwarfs (the Y dwarfs) are also being discovered in the Milky Way field by WISE (e.g., Cushing et al. 2011). Microlensing surveys have even observed a possible excess of short-duration lensing events with characteristic lens masses as low as $\sim 1 M_{Jup}$ (Sumi et al. 2011) that indicate free-floating objects in this mass regime outnumber stars in the Milky Way. Planetary-mass objects are extreme outcomes of star formation, and hence their production is a strong test of the physics of star formation.

It has long been known that the interplay between gravitational instability, turbulence, and gas opacity should allow molecular cloud fragmentation down to an opacity-limited minimum mass of $< 10 M_{Jup}$ (OLMM; Low & Lynden Bell 1976; Boss 1988). Indeed, most protostars likely begin with a first core near the OLMM (e.g., Tomida et al. 2013). However, fragments should subsequently accrete mass from the envelope and molecular cloud, growing to larger final masses. Growth can only be avoided if many prestellar clumps are much smaller than the average Jeans mass (e.g., Padoan & Nordlund 2002), if external ionization or winds disperse the protostellar envelopes quickly (e.g., Mann et al. 2015), or if cores are ejected from the natal mass reservoir (Reipurth & Clarke 2001). Ejection is disfavored based on the kinematics and spatial distribution of brown dwarfs (e.g., Luhman et al. 2009a), but the other explanations remain broadly untested. **Both hypotheses should produce IMF variations as a function of environment. Core mass should depend on gas density, temperature, and turbulence (e.g., Offner et al. 2014), and envelope dispersal will depend on the number and luminosity of nearby stars.** Given the recent evidence of IMF variations across different bulk galactic environments (Conroy & Van Dokkum 2012, though see Coulter et al. 2017), different cluster environments in the Milky Way might follow suit. IMF variations should be most apparent at the mass extrema.

Based on field objects (for stars) and young populations (for brown dwarfs), the IMF has been quantified as either a log-normal distribution (Chabrier 2003, 2005) or a twice-broken power law (Kroupa 2001), with a peak of 0.1–0.3 $M_{\odot}$. These functional forms are very similar for stars (Dabringhausen et al. 2008), but extrapolations diverge in the planetary-mass regime. The Kroupa IMF predicts that for every O star, there should be ∼90 objects with $M < 15 M_{Jup}$. The Chabrier (2005) IMF predicts only ∼5 such objects. Many brown dwarfs and a small number of planetary-mass objects have been identified from color selection and spectroscopic followup (e.g. Slesnick et al. 2008; Luhman et al. 2009b; Lodieu et al. 2013), leading to claims of other features in the substellar IMF. Drass et al. (2016) have claimed the IMF in Orion has a second peak at 25 M_{Jup}, while Gagne et al. (2015, 2017) claim a possible excess below 12 M_{Jup} in nearby young moving groups (but based on very small statistics). As we demonstrate in Figure 2, members of our team are now using Spitzer

proper motions to measure the full IMF down to 1–2 M_{Jup} in these nearby populations.

The populations in past studies were observed not because they are representative examples of star formation, but rather because they were the only feasible targets. Sparse associations (e.g. Taurus; $N_{tot} \sim 300$ members; $\rho_c \sim 5$ pc^{-3}) are extremely common and they dominate the local volume ($d < 400$ pc), but their cumulative contribution to the Milky Way's star formation rate is dwarfed by larger clusters (Lada & Lada 2003). Furthermore, these small populations are only expected to host a tiny number of extreme objects; the Chabrier (2005) log-normal IMF would predict ∼15 objects with $M \leq 15 M_{Jup}$ even in a relatively massive cluster like Orion. To understand the "typical" IMF, much less its variations, we must push toward complexes of high-mass clusters (e.g. Carina; $N_{tot} \sim 5{\times}10^4$; $\rho_c > 10^3$ pc^{-3}), probing the full range of environments and discovering enough planetary-mass objects for robust statistical tests of the IMF slope and OLMM.

These massive clusters are difficult targets for IMF studies due to their large distance, high stellar density, and location in the Galactic plane. X-ray surveys like MystiX are now uncovering the cluster populations down to $M \sim 1 M_\odot$ (e.g., Feigelson et al. 2013), mapping the upper IMF, but X-rays are insensitive to $\lesssim 0.5 M_\odot$ (Townsley et al. 2014) and do not reach the peak of the IMF ($\sim 0.2 M_\odot$). Those surveys therefore do not constrain some physics inputs, such as the turbulence from feedback that sets of the IMF turnover. Spitzer/IRAC is formally sensitive enough to reach planetary masses, but its large PSF leads to source confusion and low astrometric precision (preventing proper motion selection), and mid-IR colors do not distinguish young brown dwarfs from AGN or reddened field stars. HST lacks these limitations, offering a narrower PSF, better astrometric performance, and a larger filter complement (including specialized narrowband filters). The power of HST for cluster studies of the high-mass IMF is already being demonstrated in the most distant and extreme clusters (e.g., Westerlund 1 and the Arches; Hosek et al. 2015; Andersen et al. 2016).

HST also has limits. The camera FOVs are small ($\lesssim 2'$), and the high guide star acquisition overheads limit its mapping to 1 field per orbit. Even the densest clusters within $d \lesssim 3$ kpc are still $\gtrsim 15'$ in size, so mapping even one cluster has previously required a Large program. Several Large and Treasury programs have been approved to produce a complete panchromatic map for the nearest cluster (the Orion Nebula Cluster; $N \sim 3000$; $\rho_c \sim 100$ pc^{-3}), but the ONC is only a midsize cluster by mass. Also, the ONC programs go deep (due to long integrations and small distance), but the ONC lacks enough members to firmly identify the bottom of the IMF, and they're spread too widely for multiplexed spectroscopy.

A new observing mode (DASH, or Drift-And-SHift; Momcheva et al. 2016) now enables radically different observing programs, including efficient wide-field mapping of high-mass star clusters. DASH observing sequences map large mosaics purely under gyro control, with no need for guide star reacquisition after slews. Maps that would have required 50–200 orbits can now be executed in a third of the time, trading a modest amount of sensitivity for much wider area coverage. Given the impact of this new observing mode, now is the time to systematically map a representative sample of the best (nearest and least extincted) clusters across the cluster mass function, measuring the IMF down to 5–10 M_{Jup} and paving the way for detailed spectroscopic followup with JWST.

Our Survey: The IMF to Planetary Mass Across the Milky Way

We propose to exploit the new fast-mosaic technique with WFC3/IR to map five benchmark star-forming regions that are more massive than any in the solar neighborhood; this survey will extend our census of those clusters down the IMF into the planetary mass regime ($\sim$4–8 M_{Jup}) and across environments from sparse associations ($N \lesssim 200$ members) to massive clusters ($N \sim 5 \times 10^4$ members). We will observe each region with three filters (F110W, F139M, F160W) at three pointings per orbit with 10×25s frames per filter, efficiently mapping at a rate of 14 arcmin^2/orbit. Given their spatial extent (as judged from the extent of their OB and X-ray populations), the full survey will require 132 orbits to map all regions.

Our three-filter survey strategy will harness HST's unique position above the atmosphere in order to conclusively identify objects with late spectral types (M5–T9; Figure 5). The F139M filter is placed in the middle of the water absorption band separating the J and H atmospheric windows, and when combined with bracketing broadband filters, it yields a reddening-independent spectral index that measures the depth of absorption (Figure 3). This water index efficiently rejects reddened early-type background stars and most extragalactic contaminants, and since cluster members should sit 2–4 magnitudes above the ZAMS in a CMD using F110W and F160W (e.g., Chabrier et al. 2000), then only the foreground >M5 dwarfs within <1 kpc (Σ $\sim$2–3 arcmin^{-2} in TRILEGAL simulations; Girardi et al. 2005) will represent potential contaminants. Water filter photometry has been used with great success to identify late-type members in targeted searches of nearby populations using early NICMOS data (Najita et al. 2000) and pointed observations with WFC3/IR (Allers et al., in prep), but only the new fast-mapping mode can unlock its full potential for survey work.

We list our proposed target regions in Table 1, and outline the mosaics in Figure 4. These regions are the most heavily-studied young, massive clusters in the Milky Way, and many have a long legacy of HST imaging for smaller subfields, typically at optical wavelengths. We have specifically selected these regions to be sufficiently compact that they can be efficiently mapped (diameter $\leq 30'$), to have low foreground extinction ($A_V < 3$, or $A_H < 0.5$ and $E(J-H) < 0.5$), and to span two orders of magnitude in the cluster mass function. Since the low-mass stellar content is still poorly known in all of these regions, we parametrize the stellar mass in terms of the number of O stars, as a Chabrier IMF should produce $\sim 10^3$ members for every O star. Each region is substantially more massive than the ONC, probing a more extreme environment and massively expanding the number of known brown dwarfs and planetary-mass objects. **Massive clusters are the only place to study both extremes of the IMF; for the Chabrier (2005) IMF, each O star would denote the existence of $\sim$5 planetary-mass objects ($M \lesssim 15 M_{Jup}$).** Even the ONC is a meager hunting ground, with only 3 O stars or $\sim$15 planetary-mass objects.

We will map the entire lower IMF from $0.5 M_\odot$ to the OLMM ($\sim 5 M_{Jup}$), measuring the low-mass break, the low-mass slope, and the lower mass limit (features 6–8 in Figure 1). X-ray surveys (Feigelson et al. 2013; Townsley et al. 2014) and the O/B star census have already yielded corresponding measurements of features 3–5, and the combined results will constrain features 1–2. We therefore will end with a full IMF for a wide range of formation environments, informing the next generation of star formation models.

Our substellar and planetary-mass discoveries will be ideal targets for JWST spectroscopy. A small number of (much brighter) planetary-mass objects are being discovered in the nearest regions, but spectroscopy will be overhead-dominated, and the low spatial density prevents multiplexing. Even if the ONC's secondary IMF peak (Drass et al. 2016) is real, there are $\lesssim$100 planetary-mass objects spanning 600 arcmin^2. Westerlund 2 will host 10 times more in a third of the area, yielding many targets for multi-object spectroscopy in each $3' \times 3'$ NIRSpec/MIRI pointing. Furthermore, the HST PSF at $\lambda = 1.6\mu$m is well matched to the JWST PSF at $\lambda = 5\mu$m, so our data will reveal source confusion that would impact JWST observations in these intensely studied regions.

Additional Science Opportunities

Our proposed observations enable or improve extensive ancillary science. In particular, these fields have rich archival datasets from Spitzer (IRAC and MIPS), Chandra (the MystiX survey; Feigelson et al. 2013), and previous HST imaging. Opportunities include:

Proper Motions: We do not use proper motion selection, as these regions are distant and require time baselines of >2 years. However, a key lesson from HST is that astrometry has incredible archival value. Our data offer a crucial first epoch for future astrometric surveys of these regions; WFIRST observations in 10 years would reveal the internal kinematics and dynamical ejection rate of these benchmark populations. Furthermore, these regions have smaller subfields that were observed by previous HST instruments, and Westerlund 2 has a $4' \times 4'$ field that was observed with WFC3/IR in F110W and F160W. Given the high proper motion of Wd2 ($\sim$8 mas/yr), we can use the overlapping region to select candidates via proper motion and hence calibrate the yield of our water band search.

Circum(sub)stellar Disks: Spitzer cannot directly identify members due to source confusion and non-distinctive colors. However, HST will reveal many cluster members that do not have bright neighbors, and extant Spitzer data will identify disks for those objects. Proto-BDs typically do not display disk excesses at $\lambda < 2\mu$m (Hartmann et al. 2005), so they will not obscure the water features that we use to select candidates. However, those excesses are apparent in the IRAC bands. We will measure disk fractions from 0.2 $M_\odot$ to 5 M_{Jup}, probing planet formation across the IMF and identifying JWST spectroscopy targets.

Disk Lifetimes: Photoevaporation by the intense radiation of O stars (as exemplified by the Pillars of Creation, which fall in our M16 survey field) has been cited as one possible environmental influence for terminating planet formation and perhaps even star formation (e.g., Kroupa & Bouvier 2003). Disk surveys of the ONC and NGC 2024 (e.g., Mann et al. 2015) suggest that this might only occur in the immediate vicinity of high-mass stars, but those clusters only have 1–3 O stars. As above, the subsample of confirmed, unconfused members will test the disk fraction and properties as a function of ambient UV radiation.

Jets: Protostellar jets with [Fe II] 1.64 μm emission may be detectable in our F160W images. With the superior angular resolution of HST, Reipurth et al. (2000) identified collimated jets in wideband NICMOS images based on their morphologies alone. Jets from high-mass protostars (e.g. Reiter et al. 2015) in our WFC3 survey will quantify the jet frequency and lifetime, and identify targets for follow-up narrowband imaging and spectroscopy.

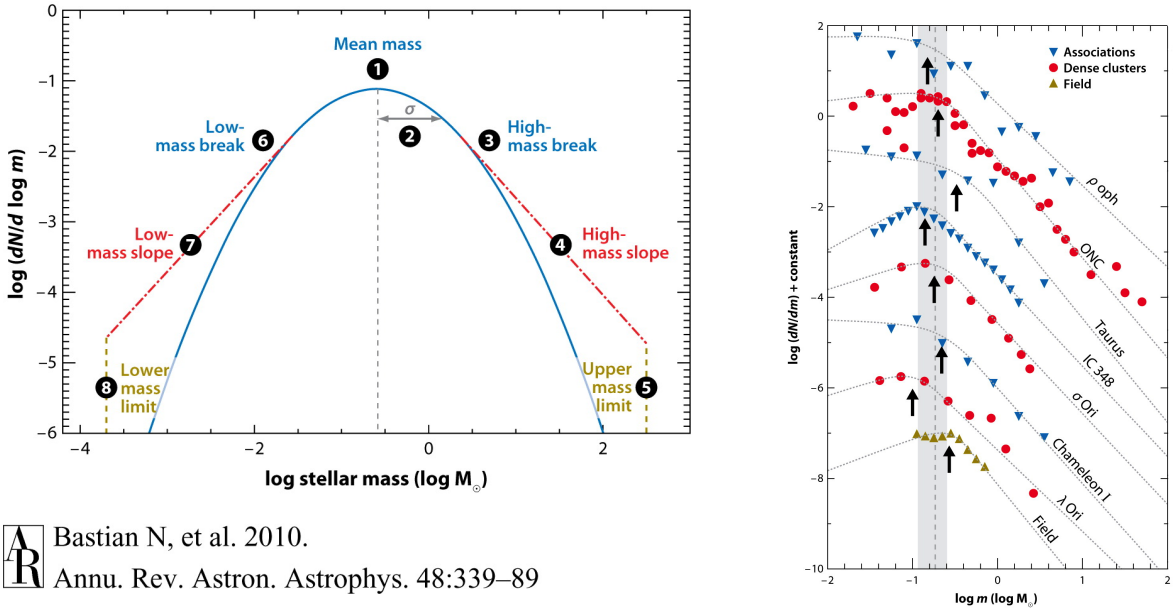

Bastian N, et al. 2010.
Annu. Rev. Astron. Astrophys. 48:339–89

Figure 1. From Bastian et al. (2010). LEFT: Schematic of the diagnostic features of the IMF. We will measure the low-mass slope (7), search for the lower mass limit (8), and compare the normalizations at low and high mass (3-5 vs 6-8). RIGHT: Mass functions derived for a sample of nearby low-mass SFRs, plus the IMF inferred from field populations. Every population here is located within $\lesssim$400 pc, and the ONC is the only cluster with >500 members. Spitzer is extending this IMF down to the planetary-mass regime in these unrepresentative local populations, but HST will be essential in testing the low-mass IMF in more typical environments.

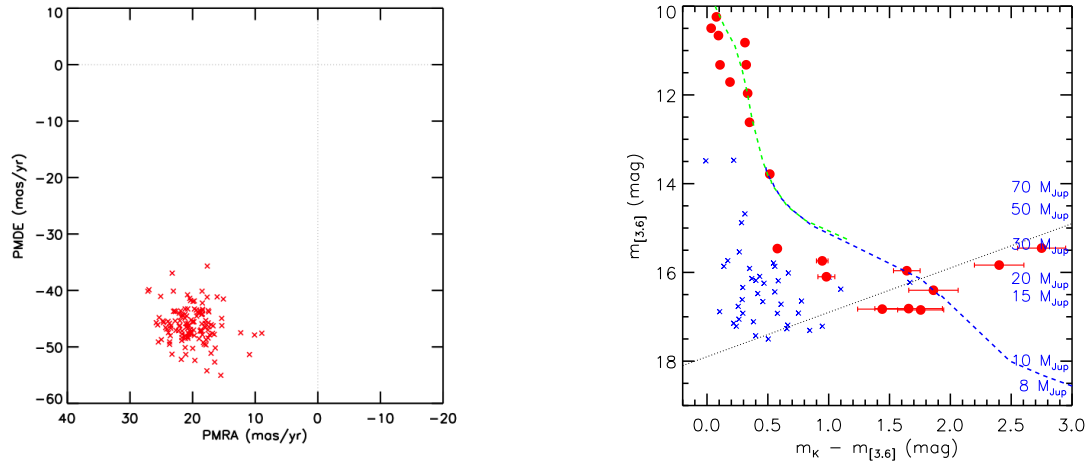

Figure 2. From Kraus et al. (2017, in prep). LEFT: Spitzer/IRAC proper motions for known Pleiades members. We have proper motions to the Spitzer flux limit for all of the nearest SFRs. Our Pleiades testbed is revealing candidates near the deuterium burning limit ($\sim 13 M_{Jup}$), despite its older age (120 Myr vs <5 Myr). RIGHT: Spitzer + UKIDSS CMD for our proper motion candidates in the Pleiades. We have found a handful of red candidates with inferred masses of 15–20 M_{Jup}. This survey is revolutionizing the IMF in nearby sparse associations, but more typical star-forming environments require the resolution and specialized water filter of HST.

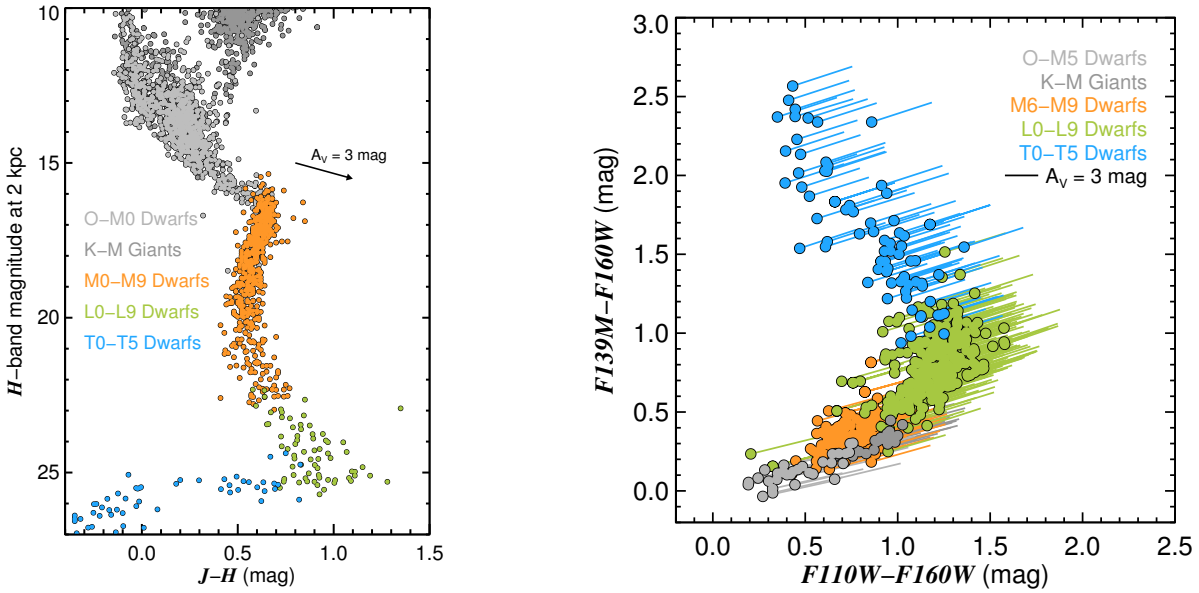

Figure 3. Modified from Bowler (2016). Color-magnitude diagram (left) and color-color diagram (right) showing the field population at $d = 2$ kpc, and a typical reddening vector we would expect in each plot. The cluster populations are likely to sit 2–3 mag above these objects in the CMD. Field early-type contaminants will redden rightward onto the CMD locus, but they will be rejected by their position in the CCD because they lack water absorption. Foreground M dwarfs will fall into the selection locus, but they can be rejected statistically due to the low surface density (∼2–3 arcmin^{-2}). There will be no M giants; they would fall outside the Milky Way.

Table 1. Benchmark Massive SFRs in the Milky Way

Region Name	Mosaic Size (′)	Dist. (pc)	Age (Myr)	A_V (mag)	# of O Stars	Orbit Cost	Main Reference
Carina (Tr14/15/16)	16×26	2300	1.1–4.8	2	65	25	Smith (2006)
RCW49+Wd2	16×16	2800	0–2	5	30	17	Zeidler et al. (2017)
M17	26×14	2000	0.7–2.4	6	14	30	Broos et al. (2007)
M16 (Eagle Neb)	24×16	1800	0.8–2.5	3	11	26	Oliveira (2008)
W3 (Main+OH)	20×30	2000	1–8	5	10	34	Kiminki et al. (2015)

The highest source density (for Carina) still corresponds to one object per 25 arcsec^2, so source confusion will not be a limiting factor. The corresponding core densities are $\rho \sim 10^3$–10^4 pc^{-3}. The age ranges (from Getman et al. 2016 or the main cluster reference) reflect the proposed spread in ages for different areas of the target populations.

NOTE: In a Chabrier (2005) IMF, for each O star ($M \gtrsim 15 M_\odot$), there are ∼120 brown dwarfs ($M < 70 M_{Jup}$) and only ∼5 planetary-mass objects ($M \lesssim 15 M_{Jup}$). To robustly identify the bottom of the IMF, we must search the most massive young clusters.

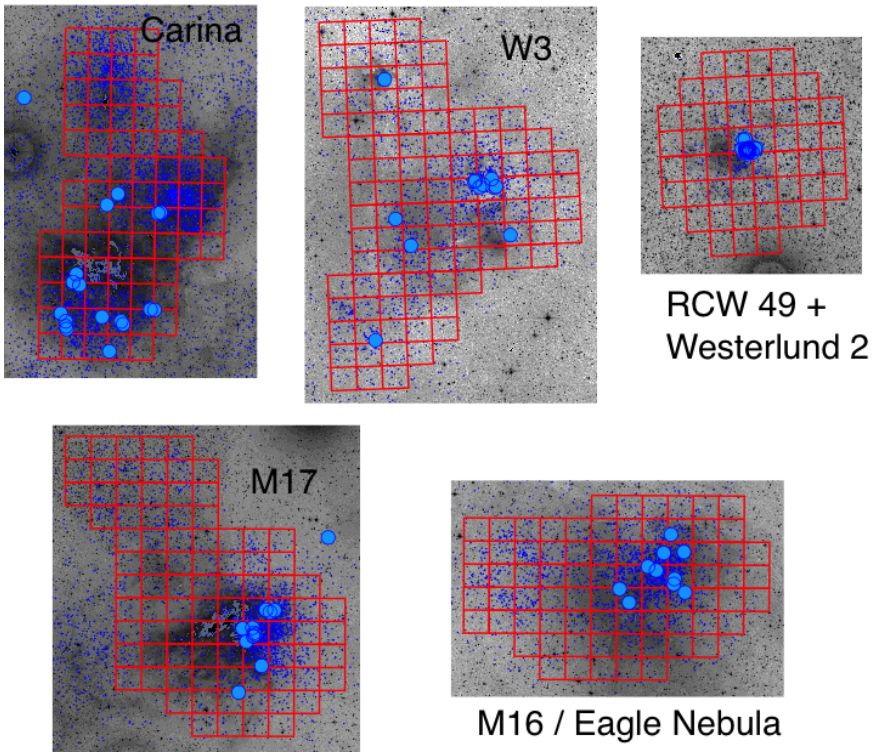

Figure 4: Maps of our target regions showing the proposed mosaics (red squares), O star population (cyan points), and known X-ray sources (blue dots), superimposed on a DSS I-band image. Our mosaic design was driven by the distribution of O stars and by the broader distribution of X-ray sources revealed by the MystiX survey (Townsley et al. 2014).

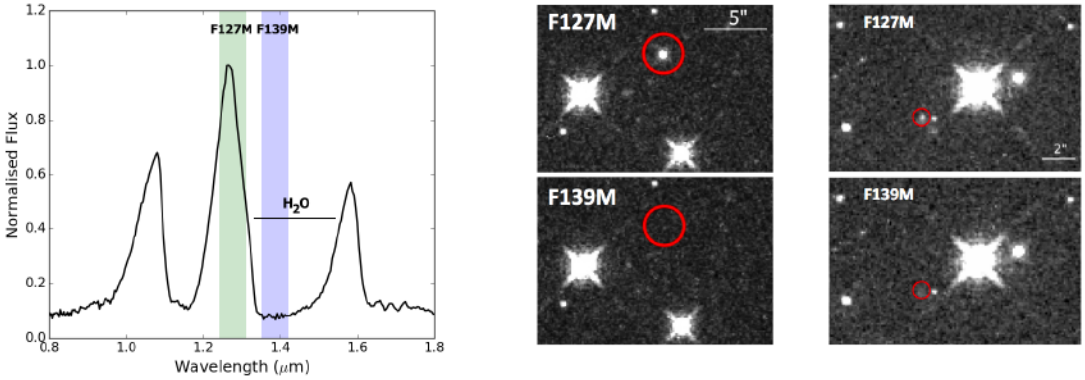

Figure 5: Examples of the power of F139M photometry for ultracool object discovery, from a program by CoIs Biller, Allers, and Fontanive. Left: SED for an ultracool dwarf, showing selection of filters to optimize color contrast in the water band. (This T dwarf is best observed with F127M; our targets are likely L dwarfs without methane absorption, so we choose F110W.) Right: Corresponding images for candidate ultracool companions to nearby stars; objects with water absorption are clear dropouts in F139M due to water absorption in their atmospheres.

Description of the Observations

Our campaign is modeled on the new observing sequences devised and verified by Momcheva et al. (2016). Traditionally, HST observing programs have been heavily penalized for adopting shallow and wide strategies, as the telescope can only move $<2'$ before new guide stars must be acquired (requiring 10 minutes or $\sim$20% of the entire orbit). The core innovation proposed by Momcheva is to avoid guide star acquisition overheads by only guiding with gyros. Even in three-gyro mode, the telescope still drifts by $\sim$1–2 milliarcseconds/sec, and hence long exposures would be compromised by smearing. However, exposure times of $<$25 sec will only be smeared by $<< \lambda/D$. For most instruments, this limit is equally onerous, as readout times are long and the data buffer is small. However, WFC3/IR uses nondestructive reads, and each read only contains the drift since the previous read. The slices of the full data cube can then be shifted and added to reconstruct a single stacked image.

We concentrate our survey on five regions (Table 1 and Figure 4) chosen to span a wide range of cluster masses and central densities, and hence to test the impact of environment on the IMF. We propose to map each cluster's full extent because mass segregation could occur quickly (or even primordially), and targeted observations of the cluster cores would bias our IMFs to preferentially exclude the least massive cluster members. Given the rarity of planetary-mass objects, we also require broad surveys in order to achieve robust statistics in every mass bin for each cluster. Since the full stellar content of these regions is not yet known, we parametrize them by the number of O+WR stars, since a Chabrier IMF would predict that 1 O star forms with $\sim 10^3$ other members. We include one cluster each from the two highest-mass categories, Carina (65 O stars) and RCW49 + Westerlund 2 (30 O stars). To match the Poisson statistics for relatively rare objects at the bottom of the IMF, we then add three representatives in a third bin: M17/Horseshoe (14 O stars), M16/Eagle (11 O stars), and W3/Main+OH (10 O stars). Our survey complements the more intensive studies of the Orion Nebula Cluster by several previous Large/Treasury programs, moving several steps up the cluster mass function with just one Large program.

Our three-filter strategy takes advantage of HST's unique vantage point above Earth's atmosphere and water vapor. H_2O is one of the strongest features in the atmospheres of ultracool dwarfs (SpT $\geq$ M5), indicating $T_{eff} \lesssim 3000$ K. By observing in F110W, F160W, and F139M, we can construct a color-color diagram (Figure 3) that measures the water absorption and controls for the effect of extinction in the ISM or the target's own molecular cloud. We will select candidate low-mass cluster members to fall on the expected cluster sequence in a color-magnitude diagram (m_{160},$m_{110}-m_{160}$), and then reject contaminants (i.e., reddened background early-type stars or AGN) based on a color-color diagram of ($m_{110} - m_{160}$,$m_{139} - m_{160}$). Our target regions are chosen for low extinction (A_V =2–6 or A_H =0.3–1.0), and reddening correction will obviate the influence of extinction variations across the cluster. Furthermore, we do not expect contamination from giants because even at the low galactic latitude of our targets, distant M giants would be outside the Milky Way. The only remaining contaminant we must plan for is foreground M dwarfs; since young members of these clusters will sit 2–3 magnitudes above the ZAMS, the contaminants will fall at smaller

distances. For a typical case like Westerlund 2, the TRILEGAL model of the Milky Way estimates the density of contaminants with $M < 0.2M_{\odot}$ (SpT $\geq$ M5) will be 2–4 arcmin^{-2}. We therefore expect $\sim$500–1000 contaminants across the entire map, while a Chabrier IMF would yield $> 10^4$ cluster members with $M < 0.2M_{\odot}$. We expect to be able to calculate membership probabilities for individual candidates based on their position on the sky and in the CMD, statistically correcting the 5–10% field contamination to measure robust IMFs.

Using APT, we have verified a modified version of the single-filter, 8-pointings-per-orbit mapping strategy from Momcheva et al. We will observe 3 pointings per orbit, which reduces the overheads due to pointing maneuvers, in 3 filters each. We can therefore obtain 9 tiles (unique filter+pointing combinations) per orbit, where all tiles use 25 s reads (SAMP-SEQ = SPARS25) and either 11 or 12 total reads (NSAMP = 11 or 12) giving total exposure times of 253 s or 278 s. No dithers are required, as each subsequent slice of the data cube is dithered by a fraction of a pixel, at no cost. The undersampled PSF is therefore realized at far more pixel phase values than in traditional dither patterns. The exposure time per tile is the minimum possible without spending on-orbit time dumping the data buffer. Only discrete read times are available with WFC3-IR, and 25 s is optimal compared to $\leq$10 s and $\geq$50 s reads. Shorter times make the data volume per orbit too large, and longer times experience too much smearing due to the pointing drift. Using NSAMP $\geq$11 allows sufficient time to dump the previous tile's datacube while exposing on the next tile. Finally, since filter changes incur much less overhead than pointing maneuvers we can fit in one more tile per orbit than the Momcheva et al. map of the COSMOS field.

Our observing strategy will yield 5σ detection limits of $m_{110W} = 25.5$, $m_{160W} = 24.2$, and $m_{139M} = 23.2$ (Vegamag). For the similar distances ($d \sim 2$ kpc) and extinctions ($A_V =$ 2–6) to all regions, our limits in F110W and F160W uniformly correspond to $\sim$3–4 M_{Jup} at $\tau = 1$ Myr or $\sim$6–8 M_{Jup} at 5 Myr (from the DUSTY models; Chabrier et al. 2000). The nominal limit for detecting ultracool dwarfs in F139M is obviously much higher, due to the large flux suppression of their water absorption bands. However, we can still reject reddened field contaminants down to the broadband limits; since the F110W and F160W detections denote source existence, then even a 2–3σ detection (as would be expected at the F160W 5σ limit) is sufficient to mark an object as a likely interloper. Even in high extinction areas ($A_V = 10$ or $A_H = 1.7$), we still expect limits of 5 M_{Jup} at 1 Myr and 10 M_{Jup} at 5 Myr.

There are several potential caveats, but none are insurmountable obstacles for our program. Star forming regions are notorious for hosting spatially resolved nebulosity, which can potentially bias both photometry and astrometry. However, the effect of this nebulosity is minimized at 1–2 μm; scattered light and line emission are signicantly fainter than the optical, but the dust is still too cool to emit thermally. HST has shown that even the Pillars of Creation (in M16) are largely transparent at NIR wavelengths. The same material also causes significant extinction, but our NIR observations are much less affected than previous optical observations. The extinction should be spatially variable, but our three-filter strategy will allow us to distinguish the effects of photospheric water absorption (which will redden only $m_{139} - m_{160}$) from extinction (which also reddens $m_{110} - m_{160}$). Extinction laws might vary, but we can use proper motions to select higher-mass members in the select regions with

past optical data, and then use those objects to test the extinction law and its variations. Finally, emission from circumstellar disks should not bias our sample because most disks around low-mass stars only contribute significant excesses at $\geq$2 μm.

Astrometry is not an immediate goal, but our observing strategy is designed to provide a high-precision first epoch for future observations with HST or WFIRST. Nondestructive reads of 25 s will only saturate on cluster stars (SpT $\sim$ M2) brighter than $V \approx 17$ mag in F139M images and $V \approx 18.5$ mag in F160W images. Gaia will provide positions and proper motions for stars brighter than $V \approx 20$ mag accurate to 0.5 mas and 0.3 mas/yr, respectively. Thus, every pointing will be able to be tied to an absolute astrometric reference frame using foreground stars, with the final accuracy likely only limited by the absolute astrometric calibration of WFC3-IR ($\sim$7 mas; ISR WFC3-2012-07). We therefore do not include overlap in our mosaics, allowing us to map for photometry in the minimum number of orbits.

Finally, shallower broadband data are available from the ground (e.g., Drass et al. 2016 for the ONC and Preibisch et al. 2011 for Carina), but they are several magnitudes shallower and lack water-band imaging (which is extremely difficult and shallow from the ground). Drass et al. (2016) show that without the discriminating power of $F139M$, the luminosity function is overwhelmed by contaminants at $K \sim 16$, far above our flux limit. Preibisch et al. (2011) used X-ray data to help, but those surveys are limited to $M > 0.5 M_{\odot}$.

Special Requirements

Our maps consist of 3 tiles per orbit over many visits. We thus specify roll angle constraints of ORIENT = 0 or 90 to ensure that tiles can be combined into a map. This is not a strict constraint as they are available for >90 days for our targets over Cycle 25.

This program is submitted as part of the **JWST Initiative**. The observations will be crucial in selecting the most scientifically compelling targets for JWST followup (highly multiplexed spectroscopy of $< 10 M_{Jup}$ objects with MIRI/NIRCam). Given the high overheads of JWST, it will be much more efficient to observe multiplexed samples of free-floating exoplanet analogs in these more distant clusters, rather than observing a single object at a time in the closer (but much less dense) star-forming regions. Furthermore, even though JWST targets could in principle be selected with Spitzer, the Spitzer PSF is an order of magnitude larger than the JWST PSF ($1.5''$ vs $0.15''$ at $\lambda = 5\mu$m). The HST PSF at $\lambda = 1.6\mu$m is well-matched to the JWST PSF at $\lambda = 5\mu$m, so our observations will reveal source confusion that would impact any JWST observations in these intensely studied regions.

Coordinated Observations

Not applicable; ancillary data from Spitzer and Chandra are already available in the archive.

Justify Duplications

We list deep broadband optical/NIR imaging, but lack space to list non-competing programs (spectra, UV, and narrowband/shallow/subarray images). All past programs only in-

clude small core fields. Young objects are variable, so we need simultaneous F110/F139/F160.

Westerlund 2

GO-10276: Two shallow pointings with WFPC2 in F336W, F439W, F555W, F814W, F656N.
GO-13038+13808: Small $4\times4'$ mosaic in cluster core with ACS (F555W, F814W, F658N) and WFC3 (F125W, F160W, F128N), plus repeat of ACS F814W. Results were reported by Zeidler et al. (2017), but they only reached a mass of $\sim$0.12 $M_\odot$.
GO-14039: An expansion of GO-13038, but only in the optical with ACS (F555W, F814W).
Summary: The GO-13808 data is similar to ours, but without F139M, it can not efficiently distinguish the lowest-mass brown dwarfs from reddened field interlopers. However, this data does present an interesting opportunity - with multiple epochs spaced by >3 years, we can verify that fast-mapping data produces robust astrometry (an untested assumption) and compare proper motion selection with water band selection in order to verify completeness.
The results of this program were reported by Zeidler et al. (2017), who did not attempt to build an IMF below 0.12 $M_\odot$. They also note that their smaller core fields are likely biased toward high-mass stars by mass segregation, which demonstrates the need for larger mosaics like our program.

M16/Eagle Nebula

GO-7117+7216: Six NIC3 pointings with F110W+F160W+narrowband (but not F139M).
GO-9091: One WFPC2 pointing with F814W and narrowband filters.
GO-9480+9488: Two ACS pure parallels in F475W and F775W.
DD-10393: Two ACS pointings in F435W, F555W, F814W, F502N, F658N
GO-10533: Mapped 1 ACS field with ACS (F775W+F850LP) and NIC2 (F110W+F160W).
GO-11981: Observed 1 WFPC2 field with F814W+F675W and UV/narrowband filters.
DD-13926: Mapped 4 WFC3 pointings with F110W+F160W, various optical narrowband.
Summary: A small number of optical pointings are available, but they would result in much shallower mass limits than our NIR observations. The small WFC3/IR mosaic lacks F139M.

M17

GO-6574: 1 WFPC2 pointing with F814W + narrowband.
GO-8992: 3 ACS pointings with F814W+F435W+narrowband.
Summary: A small number of optical pointings are available, but they would result in much shallower mass limits than our NIR observations.

W3: NONE

Carina (Tr 14/15/16)

GO-6042: 1 WFPC2 pointing with F814W+F555W+F439W+narrowband.
GO-6243+6254+7203+7786+7909+9244+9318+9676+9709+9710+10082: 24 overlapping WFPC2 pure parallels with F814W, F606W, and/or F450W.
GO-7729+7907+9269: 4 NIC3 pure parallels with F110W+F160W.
GO-9480+9575+9584+998413009: 12 ACS pure parallels with F775W
GO-10602: 2 ACS pointings with F850LP.
GO-13446+13848: 2 WFC3/IR pointings with F139M (but not F110W or F160W).
Summary: Some optical pointings are available, but they have much shallower mass limits than our NIR observations. The two WFC3/IR pointings lack F1110W and F160W.

REFERENCES

Andersen, M. et al. 2016, A&A, in press
Bastian, N. et al. 2010, ARA&A, 48, 339
Boss, A. 1988, ApJ, 331, 370
Bowler, B. 2016, PASP, 128, 2001
Broos, p. et al. 2007, ApJS, 169, 353
Chabrier, G. 2000, ApJ, 542, 464
Chabrier, G. 2003, PASP, 115, 763
Chabrier, G. 2005, "The IMF 50 Years Later", ASSL, 327, 41
Conroy, C. & van Dokkum, P. 2012, ApJ, 760, 71
Coulter, D. et al. 2017, ApJ, 835, 183
Cushing, M. et al. 2011, ApJ, 743, 50
Dabringhausen, J. et al. 2008, MNRAS, 386, 864
Drass, H. et al. 2016, MNRAS, 461, 1734
Feigelson, E. et al. 2013, ApJS, 209, 26
Gagne, J. et al. 2015, ApJS, 219, 33
Gagne, J. et al. 2017, ApJS, 228, 18
Getman, K. et al. 2017, ApJS, 229, 28
Girardi, L. et al. 2005, A&A, 436, 895
Hartmann, L. et al. 2005, ApJ, 629, 881
Hosek, M. et al. 2015, ApJ, 813, 27
Kellogg, K. et al. 2016, arXiv:1603.08529
Kiminki, M. et al. 2015, ApJ, 813, 42
Kroupa, P. 2001, MNRAS, 322, 231
Kroupa, P. & Bouvier, 2003, MNRAS, 346, 369
Lada, C. & Lada, E. 2003, ARA&A, 41, 57
Lodieu, N. et al. 2013, MNRAS, 435, 2474
Low, C. & Lynden-Bell, D. MNRAS, 176, 367
Luhman, K. et al. 2009a, ApJ, 691, 1265
Luhman, K. et al. 2009b, ApJ, 703, 399
Mann, R. et al. 2015, ApJ, 802, 77
Momcheva, I. et al. 2016, arXiv:1603.00465
Muzic, K. et al. 2015, ApJ, 810, 159
Najita, J. et al. 2000, ApJ, 541, 977
Offner, S. et al. 2014, in "Protostars and Planets VI", ed. Henrick Beuther, 53
Oliveira, J. in "Handbook of SFRs V.2", ed. B. Reipurth, 599
Padoan, P. & Nordlund, A. 2002, ApJ, 576, 870
Preibisch, T. et al. 2011, A&A, 530, 34
Reipurth, B. et al. 2000, AJ, 120, 1449
Reipurth, B. & Clarke, C. 2001, AJ, 122, 432
Reiter, M. et al. 2015, MNRAS, 448, 3429
Slesnick, C. et al. 2008, ApJ, 688, 377
Smith, N. 2006, MNRAS, 367, 763
Sumi, T. 2011, Nature, 473, 349
Tomida, K. et al. 2013, ApJ, 763, 6
Townsley, L. et al. 2014, ApJS, 213, 1
Zeidler, P. et al. 2015, AJ, 150, 78
Zeidler, P. et al. 2017, AJ, 153, 122